Quantum Dot Optomechanics in Suspended Nanophononic Strings

Anja Vogele, Maximilian M. Sonner, Benjamin Mayer, Xueyong Yuan, Matthias Weiß, Emeline D. S. Nysten, Saimon F. Covre da Silva, Armando Rastelli, and Hubert J. Krenner*

The optomechanical coupling of quantum dots and flexural mechanical modes is studied in suspended nanophononic strings. The investigated devices are designed and monolithically fabricated on an (Al)GaAs heterostructure. Radio frequency elastic waves with frequencies ranging between $f = 250$ and 400 MHz are generated as Rayleigh surface acoustic waves on the unpatterned substrate and injected as Lamb waves in the nanophononic string. Quantum dots inside the nanophononic string exhibit a 15-fold enhanced optomechanical modulation compared to those dynamically strained by the Rayleigh surface acoustic wave. Detailed finite element simulations of the phononic mode spectrum of the nanophononic string confirm that the observed modulation arises from valence band deformation potential coupling via shear strain. The corresponding optomechanical coupling parameter is quantified to 0.15 meV nm^{-1}. This value exceeds that reported for vibrating nanorods by approximately one order of magnitude at 100 times higher frequencies. Using this value, a derived vertical displacement in the range of 10 nm is deduced from the experimentally observed modulation. The results represent an important step toward the creation of large scale optomechanical circuits interfacing single optically active quantum dots with optical and mechanical waves.

Phonons are of paramount importance for the realization of hybrid quantum architectures.[1] These fundamental excitations of condensed matter couple to almost any quantum system and experience only minute dissipation in crystalline solids. Surface acoustic waves (SAWs) are one of the very few phononic technologies of industrial relevance[2] and have recently attracted widespread interest in quantum technologies. This interest has been sparked by theoretical[3–5] work and hallmark experiments on superconducting qubits.[6–8] Semiconductor quantum dots (QDs) enable the direct transduction of the SAW phonons' radio frequencies to the optical frequencies of QD excitonic two-level system[9,10] via deformation potential and Stark effect couplings.[11–13] One of the first applications of SAW envisioned and implemented in QD-based quantum technologies was the dynamic acoustic pumping and charge state control via the acousto-electric effect.[14–17] Moreover, QDs can be integrated in fully suspended photonic crystal membranes with SAW-tunable circuit elements[18,19] enabling the dynamic control of light–matter interactions at gigahertz frequencies.[20] Such suspended systems confine both photons and phonons in the plane.[21] Interestingly, flexural, anti-symmetric Lamb modes excited in these membranes are stress-neutral in the center plane of the membrane, that is, the volumetric strain vanishes. Thus, so far experiments focusing on the optomechanical coupling between QDs and mechanical excitations used samples in which the dots were deliberately displaced from the membrane's

A. Vogele, M. M. Sonner, B. Mayer, Dr. X. Yuan, M. Weiß, E. D. S. Nysten, Prof. H. J. Krenner
Lehrstuhl für Experimentalphysik 1 and Augsburg Centre for Innovative Technologies (ACIT)
Universität Augsburg
Universitätsstraße 1, 86159 Augsburg, Germany
E-mail: hubert.krenner@physik.uni-augsburg.de

Dr. X. Yuan, Dr. S. F. Covre da Silva, Prof. A. Rastelli
Institute of Semiconductor and Solid State Physics
Johannes Kepler Universität Linz
Linz Institute of Technology
Altenbergerstraße 69, 4040 Linz, Austria

M. M. Sonner, M. Weiß, E. D. S. Nysten, Prof. H. J. Krenner
Nanosystems Initiative Munich (NIM)
Schellingstraße 4, 80799 München, Germany

Prof. H. J. Krenner
Center for Nanoscience (CeNS)
Ludwig-Maximilians-Universität München
Geschwister-Scholl-Platz 1, 80539 München, Germany

**ADVANCED
SCIENCE NEWS**

www.advancedsciencenews.com

**ADVANCED
QUANTUM
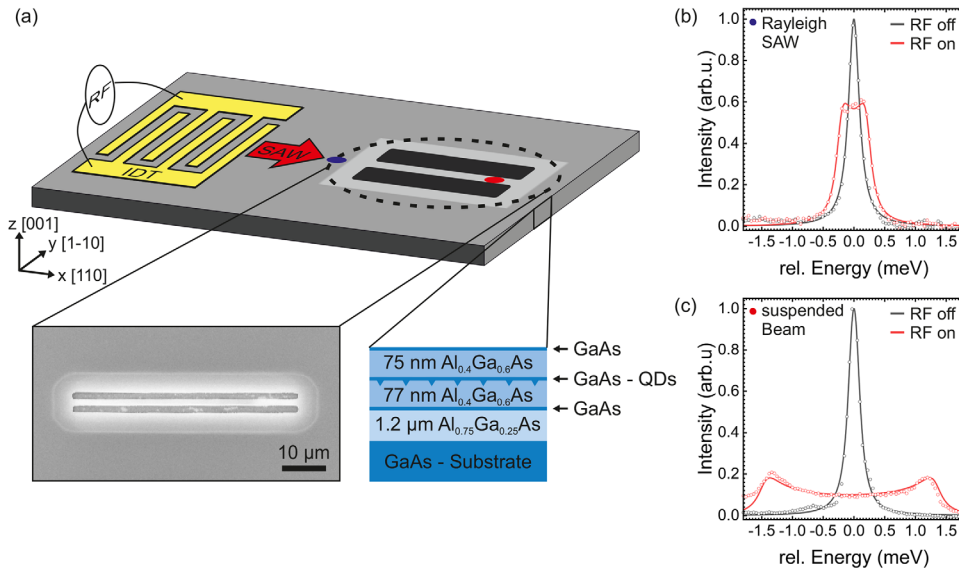TECHNOLOGIES**

www.advquantumtech.com

Figure 1. a) Sample layout consisting of a metal IDT and a 50 μm long and 2 μm wide suspended nanophononic string fabricated on an (Al,Ga)As-based heterostructure. A scanning electron microscope image of a typical nanophononic string is shown below. b,c) Emission of a single QD in the unpatterned region and inside of a nanophononic string (marked by the blue and red dot in the layout) without/with RF voltage applied to the IDT (black/red) at $f_{RF} = 370$ MHz. Solid lines are best fits of a time modulated Lorentzian (Equation (1)) to the experimental data.

center.[22–24] In contrast, further experiments showed an unexpected pronounced tuning of QDs placed in the center of the membrane[20] indicating strong optomechanical coupling of the QD exciton with modulation amplitudes comparable to that observed of a high quality factor cavity mode.

In this communication, we report on the optomechanical coupling of single GaAs/(Al)GaAs QDs to the phononic modes of suspended nanophononic strings. In the studied frequency band from $f = 250$ to 400 MHz, we observe large tuning amplitudes which are enhanced by more than a factor of 15 compared to those of QDs strained by conventional Rayleigh SAWs propagating on the unpatterned surface.

Devices were fabricated on a (Al)GaAs heterostructure containing a single layer of GaAs QDs embedded in (Al)GaAs barriers in its center. This type of QD is, in contrast to self-assembled QDs nucleating on a wetting layer,[25] not coupled to a 2D continuum of states in which acousto-electric transport could occur.[26,27] Thus, these dots are particularly suited to study strain tuning by elastic waves[28,29] since charging due to the acousto-electric effect[16,26] is almost completely suppressed. **Figure 1**a shows a schematic of the full device comprising a chirped interdigital transducer, labeled IDT, and a 50 μm long suspended nanophononic string. A scanning electron microscope image of a typical nanophononic string and the full layer sequence of the heterostructure are shown as well. Details on device fabrication can be found in the Experimental Section. When applying a radio frequency (RF) voltage to the IDT a Rayleigh SAW is generated in the unpatterned region. This Rayleigh SAW couples into the nanophononic string in which it propagates as a Lamb wave. We performed finite element model (FEM) simulation using a geometry derived from our SEM characterization. As shown in Movies M1 and M2, Supporting Information, the Rayleigh SAW is converted predominantly into an anti-symmetric, flexural Lamb mode. Figure 1b,c compares the optomechanical response

of two QDs, one in the unpatterned region [marked by blue dot in (a)] and the other inside of a nanophononic string [marked by red dot in (a)], respectively. We plot the measured photon energy, E, relative to the center energy of the unmodulated line, E_0, as symbols. The data plotted in red (black) correspond to the emission intensity of a QD transition when the RF signal is switched on (off) and the QD is (not) dynamically strained. Clearly, the emission lines show the expected broadening at both positions when the RF signal ($f_{RF} = 370$ MHz, $P_{RF} = 29$ dBm) is switched on. Most strikingly, the broadening observed for the QD inside the nanophononic string is largely enhanced compared to the QD in the unpatterned region. The observed broadening can be described by a Lorentzian line modulated in time with a frequency f_{RF}.[29–31] It is given by

$$I(E) = I_0 + f_{RF} \frac{2A}{\pi}$$

$$\times \int_0^{1/f_{RF}} \frac{w}{4 \cdot \left(E - \left(E_0 + \Delta E \cdot \sin\left(2\pi \cdot f_{RF} \cdot t \right) \right) \right)^2 + w^2} dt,$$

$$(1)$$

in which ΔE and w denote the amplitude of the optomechanical modulation and the unperturbed linewidth of the QD emission line, respectively. Best fits of Equation (1) (full lines in Figure 1b,c) faithfully reproduce the experimental data and allow us to quantify ΔE to be 0.23 and 1.40 meV for the Rayleigh SAW and on the nanophononic string, respectively. The minute offset of the center of the modulated relative to the unmodulated emission line arises most likely due to heating despite of the employed pulsed SAW excitation scheme.[20] In the Supporting Information we present stroboscopic experiments in Figure S1, Supporting Information. The data presented there confirm the
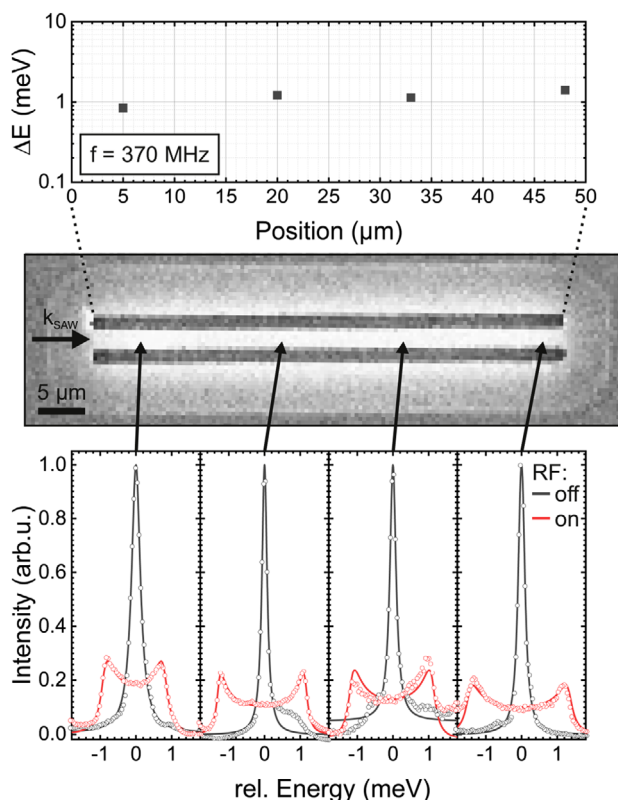
**ADVANCED
SCIENCE NEWS**

www.advancedsciencenews.com

**ADVANCED
QUANTUM
TECHNOLOGIES**

www.advquantumtech.com

Figure 2. *Lower panel:* Time-integrated emission spectra (symbols: experimental data; lines: best fits of Equation (1)) of four individual QDs located along the principal axis of the nanophononic string with (red) and without (black) a Rayleigh SAW injected. Arrows mark the positions of these dots in the SEM image in the center. *Upper panel:* Optomechanical tuning amplitude ΔE extracted from the modulated spectra of the lower panel.

conversion of the Rayleigh SAW into a flexural mode propagating in the nanophononic string.

In **Figure 2** we investigate the position dependence of the optomechanical tuning in the *x*-direction along the nanophononic string. The lower panel shows the optomechanical response of four different QDs located at different positions along the nanophononic string. Arrows indicate these positions in the SEM image in the center. Clearly, all four QDs show a clear optomechanical response when a Rayleigh SAW is injected into the string giving rise to the previously described broadening of the emission line (red symbols) compared to the unmodulated case (black symbols). Again, lines show best fits of Equation (1) to the experimental data. In the upper panel of Figure 2, we plot the optomechanical modulation amplitude ΔE as a function of position. This analysis shows that ΔE is almost independent on the position, indicating that no pronounced attenuation occurs on the 50 µm lengthscale of our strings.

Next, we analyze the frequency dependence of the optomechanical coupling in both areas. **Figure 3**a,b shows f_{RF}-dependent emission spectra of QDs strained by a Rayleigh wave (left panels) and inside a nanophononic string (right panels). The data in Figure 3a,b are recorded with a RF signal ($P_{RF} = 29$ dBm) applied by two different IDTs with designs nominally facilitating SAW excitation from $250 - 300$ and $350 - 400$ MHz, re-

spectively. The overall conversion efficiencies of theses chirped transducers is reduced compared to unchirped designs because only few finger pairs contribute to the excitation of a certain SAW frequency. The excited Rayleigh SAWs first propagate across the free, unpatterned surface and then are injected in different nanophononic strings. The normalized emission intensity is color-coded, with blue (red) corresponding to minimum (maximum) intensity, and plotted as a function of f_{RF} (vertical axis) and relative emission energy $E - E_0$ (horizontal axis). As f_{RF} is tuned, both QDs in the unpatterned region shown in Figure 3a,b exhibit weak optomechanical modulations. The modulations do not cover the full nominal frequency ranges of the IDTs due to imperfections in the nanofabrication and the aforementioned limited number of finger pairs contributing. In contrast to QDs strained by Rayleigh waves, the two dots inside the nanophononic string show strong enhancement of the optomechanical modulation over a wide frequency band. This broadband response arises from the injection of the Rayleigh wave into the nanophononic beam. Despite the acoustic impedance mismatch between Rayleigh SAWs and Lamb modes, efficient conversion is achieved[32] over the entire frequency band of the IDT. This broadband injection is in strong contrast to discrete frequency response observed for indirect coupling schemes employing sample architectures in which the nanomechanical resonator is rigidly connected to a piezoelectric actuator.[24,30,33] For the two frequency bands studied we deduce enhancements by factors of 10 and 15 with respect to the corresponding data obtained with Rayleigh SAWs, as shown in Figure 3a,b, respectively. Moreover, we detect a strong modulation between $260 - 270$ and $360 - 380$ MHz, where no modulation is observed for the QDs in the unpatterned region. Remarkably, for the frequency band studied in Figure 3b the largest modulation is observed for the QD in the nanophononic string at $f_{RF} = 266$ MHz. The extracted ΔE are plotted as a function of f_{RF} in the right panels, demonstrating the broadband enhancement of the optomechanical modulation inside the nanophononic string. This coupling is position-independent for both frequency bands as demonstrated in Figure S2, Supporting Information. We performed detailed FEM simulation of the phononic modes of the string using a geometry derived from our SEM characterization. The obtained dispersion in our 50 µm-long and 2 µm-wide string is plotted in Figure 3c. Our simulation confirms the propagation of three flexural modes which we refer to as Mode 1, Mode 2, and Mode 3. The dispersions are plotted as red, blue, and green lines in Figure 3c. Mode 1 and Mode 2 are the two fundamental flexural modes. Mode 1 has almost constant displacement across the short axis (*y*-direction) of the string which vanishes at the edges. In contrast, Mode 2 shows an inverted displacement profile with a node in the center ($y = 0$) and maximum and minimum displacement amplitude at the opposite edges. Mode 3 is the first higher order mode with two nodes along the short axis and consequently maximum/minimum displacement in the center ($y = 0$) and the edges of the string. In addition to propagating solutions, a series of bound resonances are predicted by our simulations with discrete wavevectors and frequencies. These bound solutions are marked by symbols in Figure 3c overlapped over the calculated dispersions of the propagating modes. In our experiment we couple Rayleigh SAWs into these modes and, therefore, we expect that we excite all three modes both as bound resonances as well as
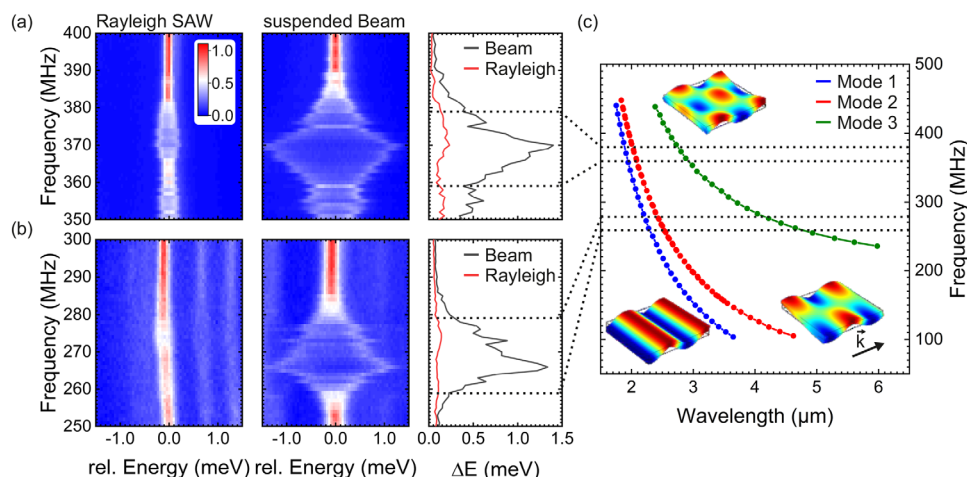
Figure 3. a,b) False-color plots of the normalized emission intensity of QDs modulated by a Rayleigh-type SAW (left panel) and inside a nanophononic string (center panel) as a function of f_{RF} and ΔE. Right Panel: Optomechanical modulation amplitude ΔE derived from the data in the other panels. The QDs embedded in a nanophononic string show an enhanced optomechanical coupling compared to the QD in the unpatterned region. c) Simulated dispersion of flexural modes of a 50 μm long and 2 μm wide suspended nanophononic string in the f_{RF} range covered in our experiment. Each data point represents one calculated stationary mode. The dotted lines mark the frequency ranges in which pronounced coupling is observed. The displacement profiles of the calculated modes are shown in the insets. The wavevector $\vec{k}$ points along the x-direction. The short axis of the string is parallel to y, perpendicular to $\vec{k}$.
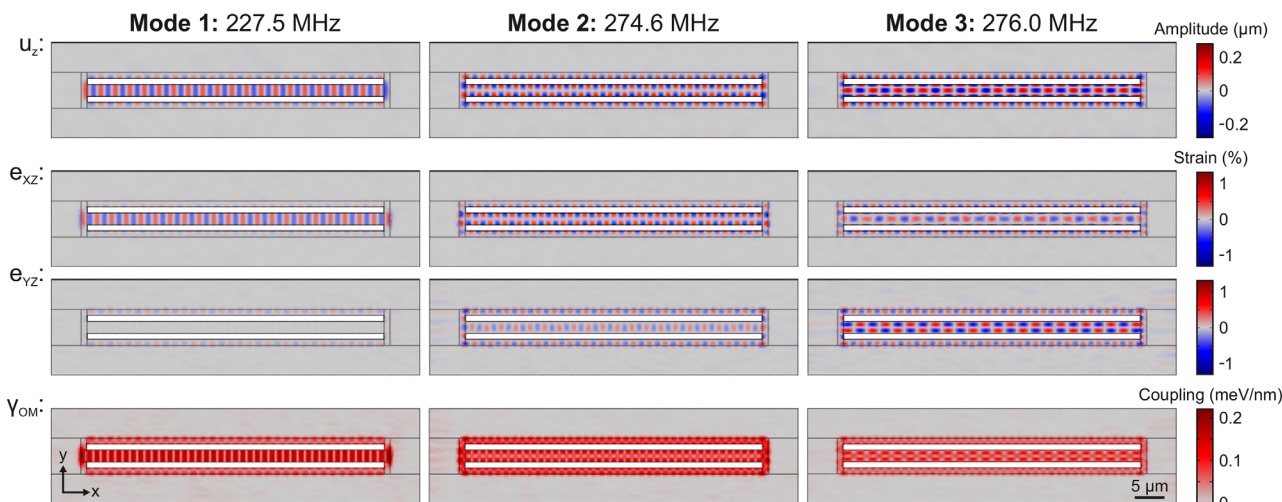

Figure 4. Simulated flexural mode profiles of the nanophononic string in the QD layer calculated by FEM. The vertical displacements u_z, shear strains components e_{xz} and e_{yz} as well as optomechanical coupling parameter γ_{OM} are depicted for the three mode profiles. As the volumetric strain vanishes at the QD layer, only shear strains of the modes contribute to the observed optomechanical tuning.

and propagating modes.[32,34] Furthermore, in the frequency band in which we observe strong enhancement of the optomechanical modulation (marked by dashed lines), our FEM simulations in Figure 3c predict multiple bound resonances for all three modes. Hence, individual resonances apparent in the data shown in the center and right panels of Figure 3a,b cannot be unambiguously attributed to certain bound resonances or disentangled from coupling to propagating modes. Moreover, we expect a strong variation of the coupling efficiency for different frequencies due to two additional effects. First, the frequency response of the IDT is not flat over the full range of frequencies and, second, the acoustic impedance mismatch between the Rayleigh SAW and Lamb waves.[32]

Nevertheless, our FEM simulations allow us to quantify the strength of optomechanical coupling for the three flexural modes. Since the center of the beam in vertical direction (z) at which the layer of QDs is located is a stress-neutral plane for flexural modes, the volumetric strain vanishes. Thus, the observed optomechanical response of the QDs has to arise from off-diagonal elements of the strain tensor (shear strain) and the corresponding deformation potentials. Deformation potential coupling by shear strain is known to be weak compared to that by the diagonal elements (normal strain). Thus, the investigation of deformation potential coupling due to shear strain is typically challenging and our experiment elegantly suppresses the dominant normal strains. In **Figure 4**, we analyze bound resonances

**ADVANCED
SCIENCE NEWS**
www.advancedsciencenews.com

**ADVANCED
QUANTUM
TECHNOLOGIES**
www.advquantumtech.com

of each of the three different modes. The upper rows show the vertical displacements (u_z) which confirm the different symmetries of the three modes. The shear strains e_{xz} and e_{yz} are plotted in the two center rows. For Mode 1, only e_{xz} is finite, while for Mode 2 and Mode 3 both shear strains contribute to the observed optomechanical tuning. Using the Pikus–Bir strain Hamiltonian and considering that the conduction band is negligibly affected by shear strains,[35] we determine the optomechanical coupling parameter to

$$\gamma_{om} = \frac{\partial E_{QD}}{\partial u_z} = d \cdot \frac{\sqrt{\left(e_{xz}^2 + e_{yz}^2\right)}}{u_z}. \qquad (2)$$

Because the center of the nanostring is a stress-neutral plane, Equation (2) only contains the valence band deformation potential d and the shear strain tensor components e_{xz} and e_{yz}. Using our FEM simulations and Equation (2) we are able to directly evaluate γ_{om} for all three modes using the bulk value of the deformation potential of GaAs, $d = -4.8$ eV.[36] The obtained profiles are plotted in the bottom row of Figure 4. Our simulations predict the largest $\gamma_{om} \approx 0.2$ meV nm^{-1} for Mode 1 and $\gamma_{om} \approx 0.1 - 0.15$ meV nm^{-1} for Mode 2 and Mode 3. As expected, these values are approximately one order of magnitude smaller than that for Rayleigh waves, for which strong normal (volumetric) strain dominates.[9,28] However, the values obtained are about one order of magnitude larger than that reported for vibrating nanowires[30,33] at more than two orders of magnitude higher frequencies. From our simulations we can also quantify the displacements corresponding to the values of ΔE observed in our experiment. The maxima $\Delta E = 1.401$ meV at $f_{RF} = 370$ MHz and 1.336 meV at $f_{RF} = 266$ MHz in Figure 3a,b correspond to $u_z = 10.5 \pm 3.5$ nm and 10.0 ± 3.4 nm, respectively. Analogous analysis of the data for Rayleigh waves yields $u_z = 0.08$ nm ($\gamma_{om} \approx 2.89$ meV nm^{-1}) and 0.04 nm ($\gamma_{om} \approx 2.08$ meV nm^{-1}) at these frequencies. The strong enhancement of u_z in the nanophononic string is a direct consequence of the localization of mechanical energy in this fully suspended structure and that the string can freely oscillate, in contrast to the Rayleigh wave.

In conclusion, we demonstrate that QDs can be coupled to flexural modes of a suspended nanophononic string and observe a strong enhancement of the optomechanically induced spectral modulation at radio frequencies exceeding 400 MHz, important to reach the resolved sideband regime.[10] In this regime parametric transduction becomes accessible and enables the implementation of hybrid quantum dot optomechanical transduction and control schemes. Our scheme could be also applied to QD-molecules to dynamically switch coupling of charge and spin excitation by strain. Furthermore, our scheme can be directly applied to exciton and spin qubits of QD molecules[37–42] or of optically active defect centers,[43–45] for which recent proposals[46–48] promise high fidelity quantum control schemes, or QDs forming in nanowires.[12,13,17,49,50] Moreover, our work marks a first important step to interface optomechanical crystals with engineered dispersions of phonons and photons and operation frequencies in the GHz domain.[51,52] Finally, the observed optomechanical coupling arises exclusively from shear strain modulating the valence band of the semiconductor, a rarely studied effect compared to normal strain coupling.

Experimental Section

Sample Design: The (Al)GaAs heterostructure consists of the following layer sequence (beginning from the GaAs substrate in z-direction): a 1.2 µm thick Al$_{0.8}$Ga$_{0.2}$As sacrificial layer, a 4 nm thick GaAs layer followed by a 77 nm thick Al$_{0.4}$Ga$_{0.6}$As layer, the GaAs QD layer obtained by filling with 2 nm GaAs droplet-etched nanoholes, a 75 nm thick Al$_{0.4}$Ga$_{0.6}$As layer, and a 4 nm GaAs think layer.

First, multi-passband IDTs were fabricated in a standard lift-off process[31] using a Cr/Au (5 nm/50 nm) metallization which is inert to hydrofluoric acid (HF) etching employed to release the nanophononic strings.

Second, nanophononic strings were fabricated in a top-down process. The beam pattern was defined by electron beam lithography and transferred using ICP-RIE using a BCl$_3$/Cl$_2$/Ar process, and undercut was obtained by selective HF etching and critical point drying. After underetching, the QDs are located in the middle of the nanobeam along the growth direction and the two 4 nm thick GaAs layers protect the Al-containing strings from oxidation.

Acousto-Optical Spectroscopy: QDs are studied by conventional low temperature ($T = 10$ K) microphotoluminescence (µ-PL) spectroscopy. Rayleigh SAWs are generated on the unpatterned heterostructure by a signal generator connected to the IDTs. The SAW is generated in short pulses to suppress unwanted heating of the sample.[20] Furthermore, the laser exciting the µ-PL is synchronized with the electrically generated SAW pulses by a delay generator to probe the QDs only when the acoustic wave is present. In stroboscopic experiments the laser repetition rate was commensurate to f_{RF} and the relative phase was tuned.[18,53]

Numerical Simulations: The phononic mode spectrum was calculated using COMSOL Multiphysics using a tetrahedral mesh and bulk mechanical properties of all materials of the heterostructure. The geometry for simulations comprises in vertical direction the nominal heterostructure and in the plane the shape of the string and the adjacent undercut area as derived from optical microscope and SEM images.

Supporting Information

Supporting Information is available from the Wiley Online Library or from the author.

Acknowledgements

Conflict of Interest

The authors declare no conflict of interest.

Keywords

**ADVANCED
SCIENCE NEWS**

www.advancedsciencenews.com

**ADVANCED
QUANTUM
TECHNOLOGIES**

www.advquantumtech.com

[1] G. Kurizki, P. Bertet, Y. Kubo, K. Mølmer, D. Petrosyan, P. Rabl, J. Schmiedmayer, *Proc. Natl. Acad. Sci. USA* **2015**, *112*, 3866.

[2] P. Delsing, A. N. Cleland, M. J. A. Schuetz, J. Knörzer, G. Giedke, J. I. Cirac, K. Srinivasan, M. Wu, K. C. Balram, C. Bäuerle, T. Meunier, C. J. B. Ford, P. V Santos, E. Cerda-Méndez, H. Wang, H. J. Krenner, E. D. S. Nysten, M. Weiß, G. R. Nash, L. Thevenard, C. Gourdon, P. Rovillain, M. Marangolo, J.-Y. Duquesne, G. Fischerauer, W. Ruile, A. Reiner, B. Paschke, D. Denysenko, D. Volkmer et al., *J. Phys. D: Appl. Phys.* **2019**, *52*, 353001.

[3] R. Blattmann, H. J. Krenner, S. Kohler, P. Hänggi, *Phys. Rev. A* **2014**, *89*, 012327.

[4] M. J. A. Schuetz, E. M. Kessler, G. Giedke, L. M. K. Vandersypen, M. D. Lukin, J. I. Cirac, *Phys. Rev. X* **2015**, *5*, 031031.

[5] M. J. A. Schuetz, J. Knörzer, G. Giedke, L. M. K. Vandersypen, M. D. Lukin, J. I. Cirac, *Phys. Rev. X* **2017**, *7*, 041019.

[6] M. V. Gustafsson, T. Aref, A. F. Kockum, M. K. Ekstrom, G. Johansson, P. Delsing, *Science* **2014**, *346*, 207.

[7] A. Bienfait, K. J. Satzinger, Y. P. Zhong, H.-S. Chang, M.-H. Chou, C. R. Conner, É. Dumur, J. Grebel, G. A. Peairs, R. G. Povey, A. N. Cleland, *Science* **2019**, *364*, 368.

[8] B. A. Moores, L. R. Sletten, J. J. Viennot, K. W. Lehnert, *Phys. Rev. Lett.* **2018**, *120*, 227701.

[9] M. Weiß, H. J. Krenner, *J. Phys. D: Appl. Phys.* **2018**, *51*, 373001.

[10] M. Metcalfe, S. M. Carr, A. Muller, G. S. Solomon, J. Lawall, *Phys. Rev. Lett.* **2010**, *105*, 37401.

[11] J. R. Gell, M. B. Ward, R. J. Young, R. M. Stevenson, P. Atkinson, D. Anderson, G. A. C. Jones, D. A. Ritchie, A. J. Shields, *Appl. Phys. Lett.* **2008**, *93*, 081115.

[12] M. Weiß, J. B. Kinzel, F. J. R. Schülein, M. Heigl, D. Rudolph, S. Morkötter, M. Döblinger, M. Bichler, G. Abstreiter, J. J. Finley, G. Koblmüller, A. Wixforth, H. J. Krenner, *Nano Lett.* **2014**, *14*, 2256.

[13] M. Weiß, F. J. R. Schülein, J. B. Kinzel, M. Heigl, D. Rudolph, M. Bichler, G. Abstreiter, J. J. Finley, A. Wixforth, G. Koblmüller, H. J. Krenner, *J. Phys. D: Appl. Phys.* **2014**, *47*, 394011.

[14] C. Wiele, F. Haake, C. Rocke, A. Wixforth, *Phys. Rev. A* **1998**, *58*, R2680.

[15] O. D. D. Couto, S. Lazić, F. Iikawa, J. A. H. Stotz, U. Jahn, R. Hey, P. V. Santos, *Nat. Photonics* **2009**, *3*, 645.

[16] F. J. R. Schülein, K. Müller, M. Bichler, G. Koblmüller, J. J. Finley, A. Wixforth, H. J. Krenner, *Phys. Rev. B* **2013**, *88*, 085307.

[17] A. Hernández-Mínguez, M. Möller, S. Breuer, C. Pfüller, C. Somaschini, S. Lazić, O. Brandt, A. García-Cristóbal, M. M. de Lima, A. Cantarero, L. Geelhaar, H. Riechert, P. V Santos, *Nano Lett.* **2012**, *12*, 252.

[18] D. A. Fuhrmann, S. M. Thon, H. Kim, D. Bouwmeester, P. M. Petroff, A. Wixforth, H. J. Krenner, *Nat. Photonics* **2011**, *5*, 605.

[19] S. Kapfinger, T. Reichert, S. Lichtmannecker, K. Müller, J. J. Finley, A. Wixforth, M. Kaniber, H. J. Krenner, *Nat. Commun.* **2015**, *6*, 8540.

[20] M. Weiß, S. Kapfinger, T. Reichert, J. J. Finley, A. Wixforth, M. Kaniber, H. J. Krenner, *Appl. Phys. Lett.* **2016**, *109*, 033105.

[21] E. Gavartin, R. Braive, I. Sagnes, O. Arcizet, A. Beveratos, T. J. Kippenberg, I. Robert-Philip, *Phys. Rev. Lett.* **2011**, *106*, 203902.

[22] S. G. Carter, A. S. Bracker, M. K. Yakes, M. K. Zalalutdinov, M. Kim, C. S. Kim, C. Czarnocki, M. Scheibner, D. Gammon, *Appl. Phys. Lett.* **2017**, *111*, 183101.

[23] S. G. Carter, A. S. Bracker, G. W. Bryant, M. Kim, C. S. Kim, M. K. Zalalutdinov, M. K. Yakes, C. Czarnocki, J. Casara, M. Scheibner, D. Gammon, *Phys. Rev. Lett.* **2018**, *121*, 246801.

[24] X. Yuan, M. Schwendtner, R. Trotta, Y. Huo, J. Martín-Sánchez, G. Piredda, H. Huang, J. Edlinger, C. Diskus, O. G. Schmidt, B. Jakoby, H. J. Krenner, A. Rastelli, *Appl. Phys. Lett.* **2019**, *115*, 181902.

[25] D. Leonard, K. Pond, P. M. Petroff, *Phys. Rev. B* **1994**, *50*, 11687.

[26] S. Völk, F. J. R. Schülein, F. Knall, D. Reuter, A. D. Wieck, T. A. Truong, H. Kim, P. M. Petroff, A. Wixforth, H. J. Krenner, *Nano Lett.* **2010**, *10*, 3399.

[27] S. Völk, F. Knall, F. J. R. Schülein, T. A. Truong, H. Kim, P. M. Petroff, A. Wixforth, H. J. Krenner, *Nanotechnology* **2012**, *23*, 285201.

[28] F. J. R. Schülein, E. Zallo, P. Atkinson, O. G. Schmidt, R. Trotta, A. Rastelli, A. Wixforth, H. J. Krenner, *Nat. Nanotechnol.* **2015**, *10*, 512.

[29] E. D. S. Nysten, Y. H. Huo, H. Yu, G. F. Song, A. Rastelli, H. J. Krenner, *J. Phys. D: Appl. Phys.* **2017**, *50*, 43LT01.

[30] I. Yeo, P.-L. de Assis, A. Gloppe, E. Dupont-Ferrier, P. Verlot, N. S. Malik, E. Dupuy, J. Claudon, J.-M. Gérard, A. Auffèves, G. Nogues, S. Seidelin, J.-P. Poizat, O. Arcizet, M. Richard, *Nat. Nanotechnol.* **2014**, *9*, 106.

[31] M. Weiß, A. L. Hörner, E. Zallo, P. Atkinson, A. Rastelli, O. G. Schmidt, A. Wixforth, H. J. Krenner, *Phys. Rev. Appl.* **2018**, *9*, 014004.

[32] A. V. Korovin, Y. Pennec, M. Stocchi, D. Mencarelli, L. Pierantoni, T. Makkonen, J. Ahopelto, B. Djafari Rouhani, *J. Phys. D: Appl. Phys.* **2019**, *52*, 32LT01.

[33] M. Montinaro, G. Wüst, M. Munsch, Y. Fontana, E. Russo-Averchi, M. Heiss, A. Fontcuberta i Morral, R. J. Warburton, M. Poggio, *Nano Lett.* **2014**, *14*, 4454.

[34] Y. Takagaki, E. Wiebicke, P. V Santos, R. Hey, K. H. Ploog, *Semicond. Sci. Technol.* **2002**, *17*, 1008.

[35] P. Y. Yu, M. Cardona, *Fundamentals of Semiconductors: Physics and Material Properties*, Springer, Berlin **2005**.

[36] I. Vurgaftman, J. R. Meyer, L. R. Ram-Mohan, *J. Appl. Phys.* **2001**, *89*, 5815.

[37] H. J. Krenner, S. Stufler, M. Sabathil, E. C. Clark, P. Ester, M. Bichler, G. Abstreiter, J. J. Finley, A. Zrenner, *New J. Phys.* **2005**, *7*, 184.

[38] H. J. Krenner, E. C. Clark, T. Nakaoka, M. Bichler, C. Scheurer, G. Abstreiter, J. J. Finley, *Phys. Rev. Lett.* **2006**, *97*, 76403.

[39] A. Greilich, S. G. Carter, D. Kim, A. S. Bracker, D. Gammon, *Nat. Photonics* **2011**, *5*, 702.

[40] K. Müller, A. Bechtold, C. Ruppert, C. Hautmann, J. S. Wildmann, T. Kaldewey, M. Bichler, H. J. Krenner, G. Abstreiter, M. Betz, J. J. Finley, *Phys. Rev. B* **2012**, *85*, 241306.

[41] E. Zallo, R. Trotta, V. Křápek, Y. H. Huo, P. Atkinson, F. Ding, T. Šikola, A. Rastelli, O. G. Schmidt, *Phys. Rev. B* **2014**, *89*, 241303.

[42] S. G. Carter, A. S. Bracker, M. K. Yakes, M. K. Zalalutdinov, M. Kim, C. S. Kim, B. Lee, D. Gammon, *Nano Lett.* **2019**, *19*, 6166.

[43] D. A. Golter, T. Oo, M. Amezcua, I. Lekavicius, K. A. Stewart, H. Wang, *Phys. Rev. X* **2016**, *6*, 041060.

[44] S. J. Whiteley, G. Wolfowicz, C. P. Anderson, A. Bourassa, H. Ma, M. Ye, G. Koolstra, K. J. Satzinger, M. V. Holt, F. J. Heremans, A. N. Cleland, D. I. Schuster, G. Galli, D. D. Awschalom, *Nat. Phys.* **2019**, *15*, 490.

[45] F. Iikawa, A. Hernández-Mínguez, I. Aharonovich, S. Nakhaie, Y.-T. Liou, J. M. J. Lopes, P. V. Santos, *Appl. Phys. Lett.* **2019**, *114*, 171104.

[46] G. Calajó, M. J. A. Schuetz, H. Pichler, M. D. Lukin, P. Schneeweiss, J. Volz, P. Rabl, *Phys. Rev. A* **2019**, *99*, 053852.

[47] M.-A. Lemonde, S. Meesala, A. Sipahigil, M. J. A. Schuetz, M. D. Lukin, M. Loncar, P. Rabl, *Phys. Rev. Lett.* **2018**, *120*, 213603.

[48] M. C. Kuzyk, H. Wang, *Phys. Rev. X* **2018**, *8*, 041027.

[49] S. Lazić, E. Chernysheva, A. Hernández-Mínguez, P. V Santos, H. P. van der Meulen, *J. Phys. D: Appl. Phys.* **2018**, *51*, 104001.

[50] S. Lazić, E. Chernysheva, Ž. Gačević, H. P. van der Meulen, E. Calleja, J. M. Calleja Pardo, *AIP Adv.* **2015**, *5*, 097217.

[51] M. Eichenfield, J. Chan, R. M. Camacho, K. J. Vahala, O. Painter, *Nature* **2009**, *462*, 78.

[52] K. C. Balram, M. I. Davanço, J. D. Song, K. Srinivasan, *Nat. Photonics* **2016**, *10*, 346.

[53] S. Völk, F. Knall, F. J. R. Schülein, T. A. Truong, H. Kim, P. M. Petroff, A. Wixforth, H. J. Krenner, *Appl. Phys. Lett.* **2011**, *98*, 023109.